

## *International Journal of Scientific Research and Reviews*

### **DC conductivity of nanocrystalline calcium tungstate**

**Ananda Kumar V M**\*

Nanomaterials Lab, Department of Physics and Research Centre  
Mahatma Gandhi College, Pattom P O, Thiruvananthapuram, Kerala PIN 695004, India  
e-mail: [anandmgc@gmail.com](mailto:anandmgc@gmail.com) Mob. No. 09447304866

#### **ABSTRACT**

Nanostructured materials exhibit novel properties which can be tuned to specific needs for technological application. This can be often ascribed to the presence of large number of surface atoms in nanograined materials. Often grain boundaries present a large number of defects such as vacancies, dangling bonds etc. which play a vital role in determining the transport properties of nanocrystalline materials. Band structure modification resulting from nanostructuring, trapping of charged carriers in the nanograins and the large contribution from surface atoms with defective structure affects the electrical properties of nanomaterials in a large way. In the present study nanostructured calcium tungstate ( $\text{CaWO}_4$ ) of different grain sizes were synthesized using controlled chemical precipitation technique. The presence of subphases was identified using differential thermal analysis. The crystal structure and grain size were determined from the X-ray diffraction pattern of the samples. The contribution to x-ray line broadening from strain was eliminated using Hall-Williamson analysis. The interplanar spacing and grain size distribution were also ascertained using transmission electron microscopy. The dc electrical conductivity of compacts of nanocrystalline  $\text{CaWO}_4$  were studied as a function of temperature. The variation of dc electrical conductivity with chamber pressure, grain size and low temperature annealing were studied.

**KEYWORDS:** Calcium tungstate, electrical conductivity, nanostructured materials, transmission electron microscopy, X-ray diffraction.

#### **\*Corresponding Author**

**Ananda Kumar V M**

Nanomaterials Lab,

Department of Physics and Research Centre

Mahatma Gandhi College,

Pattom P O, Thiruvananthapuram,

Kerala PIN 695004, India

E-mail: [anandmgc@gmail.com](mailto:anandmgc@gmail.com) Mob: 09447304866

## INRODUCTION

Nanostructured materials often exhibit properties that are drastically different from those of conventional coarse grained counter parts<sup>1-5</sup>. In many cases, this can be attributed to large fraction of grain boundaries and hence large number of surface atoms. These grain boundaries contain a high density of defects such as vacancies, dangling bonds etc. which can control the transport properties of nanocrystalline materials in a significant way. The variations in electrical properties of nanocrystalline materials compared to conventional bulk material are ascribed to the modification of band structure, quantum confinement of charge carriers and the enhanced contributions from largely defective and strained grain boundaries as a result of nanostructuring<sup>6-10</sup>.

It has been observed experimentally that grain size significantly affect the formation of defects and influence the transport properties of pure nanocrystalline CeO<sub>2</sub>. The reduction in grain size to nanosize results in lowering of resistance per grain boundary. It is also reported that electrical resistance of nanocrystalline Ni-P alloys is considerably altered compared to amorphous alloys<sup>11-12</sup>. It is reported that in the case of nanocrystalline cobalt ferrite the dc conductivity decreases when the grain size is increased from 8 to 92 nm. The experimentally observed changes in the dc conductivity have been attributed to the changes in the cation distribution and to the increase in grain size. The observed decrease in dc conductivity with increase in grain size is explained as due to the migration of Fe<sup>3+</sup> ions from octahedral to tetrahedral sites as a result of thermal annealing<sup>13</sup>. In the case of semiconductor nanoparticles a reduction in the value of conductivity is expected due to the increase in the width of the forbidden gap which is a well known phenomenon called quantum size effect prevalent in nanostructured materials<sup>6,14-15</sup>. But in semiconductor nanoparticles, lattice defects may create donor or acceptor levels between the conduction and valance bands resulting in trapping of charge carriers<sup>6,14</sup>. This can profoundly affect the electrical response of semiconductor nanostructures. Significant increase in the electrical conductivity is observed in the case of nanostructured CdS and ZnS compared to their bulk counterparts<sup>14</sup>.

In the case of nanostructured NiO, it is reported that the conductivity of the samples was found to be enhanced by six to eight orders of magnitude over that of single crystals<sup>6, 16</sup>. This enhancement in conductivity is explained as due to the high density of Ni<sup>2+</sup> vacancies in the nanoparticle samples. The dc electrical resistivity of compacted nanoparticle assembly of Cu<sub>2</sub>O and its variation with temperature is reported in the literature<sup>17,18</sup>. The variation of dc resistivity with temperature has been explained on the basis of variable range hopping conduction between Cu<sup>+</sup> and Cu<sup>2+</sup> ions at the interfaces of Cu<sub>2</sub>O nanocrystals. Grain size dependent electrical transport properties

of nanocrystalline ZnO can be exploited effectively to employ it as a gas sensor at low temperatures<sup>19-20</sup>.

CaWO<sub>4</sub> belongs to scheelite family and each molecule consists of Ca<sup>2+</sup> cation and WO<sub>4</sub><sup>2-</sup> oxoanion with homopolar bonding<sup>21</sup>. Investigations on nanoparticles of CaWO<sub>4</sub> indicate that the optical properties may be explained in terms of the transitions in the oxocomplex states alone<sup>22,23</sup>. The ac conductivity measurements performed on single crystals of PbMoO<sub>4</sub> indicates that at low temperatures the conduction is predominantly ionic whereas at higher temperatures the contribution of the electronic conduction increases<sup>24</sup>. Despite the tetragonal symmetry of scheelites, no anisotropic conduction was observed in single crystals of PbMoO<sub>4</sub><sup>24</sup>. Investigations on single crystals of CaWO<sub>4</sub> also do not show any anisotropy in electrical conductivity. Ringdon and Grace<sup>25</sup> studied the electrical conductivity of CaWO<sub>4</sub> at 900-1300 °C and partial pressures of oxygen from 10<sup>-9</sup> to 10<sup>-14</sup> atm. The tungstate was found to be an *n*-type semiconductor and its defect structure was interpreted in terms of oxygen vacancies and interstitials. The conductivity mechanism in molybdates and tungstates are largely unexplored and very few reports are found in the literature. In the present study, nanostructured samples of CaWO<sub>4</sub> with two different grain sizes were synthesized using chemical precipitation technique and dc conductivity of these samples in compacted form are studied.

## EXPERIMENTAL

Nanoparticles of calcium tungstate were synthesized using calcium chloride dihydrate (CaCl<sub>2</sub> · 2H<sub>2</sub>O) and sodium tungstate dihydrate (Na<sub>2</sub>WO<sub>4</sub> · 2H<sub>2</sub>O). The precipitate obtained was separated and washed several times with distilled water and with acetone. The precipitate was dried in an oven at a temperature of ~100 °C and finely powdered using an agate mortar. Nanoparticles of CaWO<sub>4</sub> of two different grain sizes were prepared by changing the reaction temperature, solvent and concentrations of the reactants.

In order to ascertain the presence of subphases and purity of the synthesized nanoparticle samples, differential thermal analysis (DTA) of nanoparticles of CaWO<sub>4</sub> samples of the lowest grain size was carried out. The DTA was performed using oxygen as the purge gas in the temperature range 30 to 1200 °C at a heating rate of 10 °C per minute. The DTA curve corresponding to sample of lowest grain size of nanoparticles of CaWO<sub>4</sub> are shown in figure 1. The DTA curve of nanoparticle sample of CaWO<sub>4</sub> shows a peak at 1068 °C. This illustrates that the nanoparticle sample of CaWO<sub>4</sub> is stoichiometric and it is devoid of any subphases.

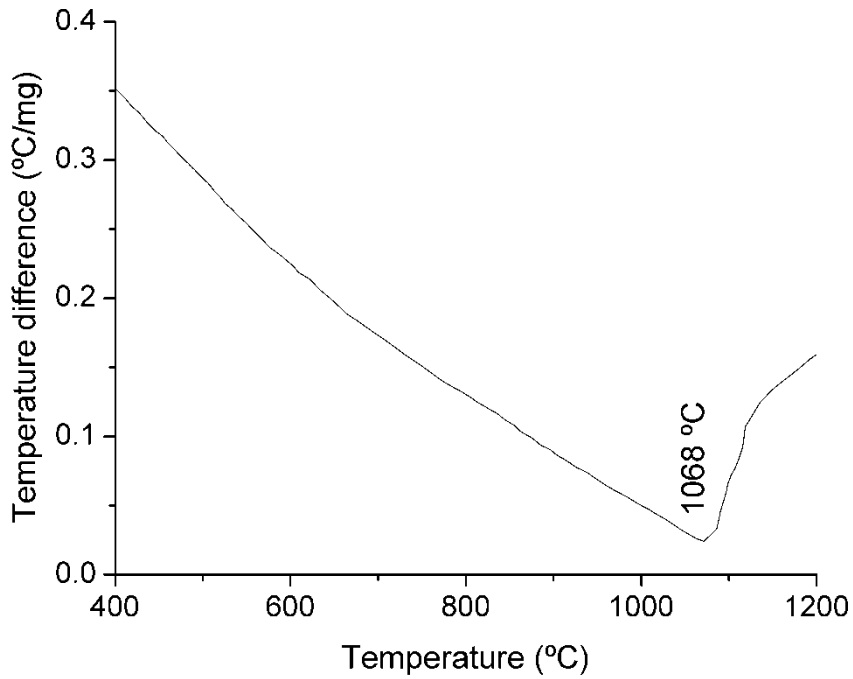


Figure 1 DTA curve of nanocrystalline CaWO<sub>4</sub>

## RESULTS AND DISCUSSION

Figure 2 shows the x-ray diffraction (XRD) pattern of one of the samples of as prepared nanocrystalline sample of CaWO<sub>4</sub>. The diffraction peaks in the XRD pattern can be indexed to scheelite structured CaWO<sub>4</sub> (ICDD data file No. 41-1431). The average grain size can be determined from the broadening of x-ray diffraction peaks using Scherrer equation. The Scherrer equation is

$$D = k \lambda / \beta \cos \theta \quad (1)$$

where D is the crystallite size ( $\text{\AA}$ ),  $k = 0.9$  is a constant related to the crystallite shape,  $\lambda$  is the wavelength of radiation used,  $\theta$  is the diffraction angle and  $\beta$  is the full-width-at-half-maximum (FWHM) of the diffraction line at  $2\theta$ .

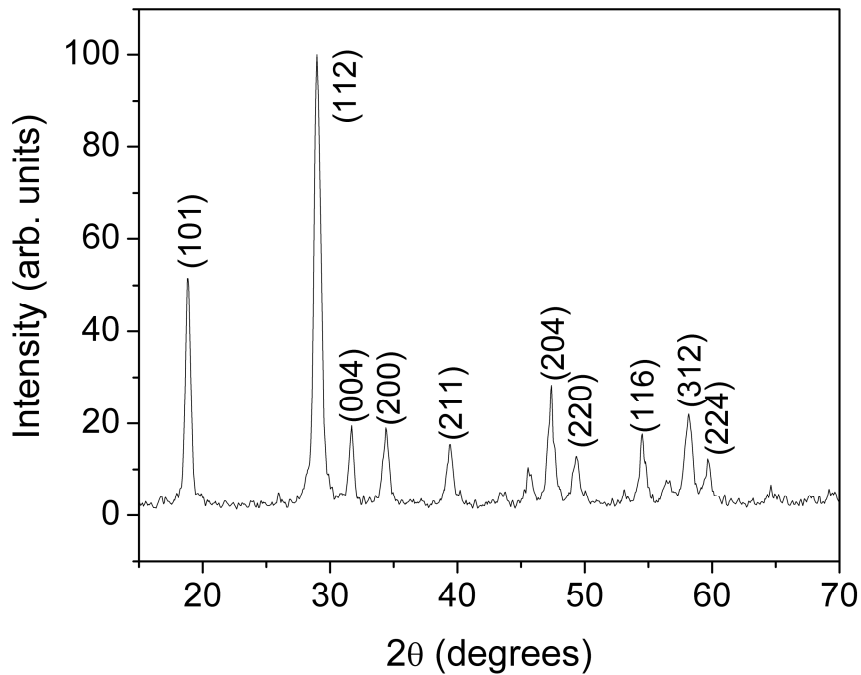


Figure 2 XRD pattern of nanocrystalline  $\text{CaWO}_4$

In deriving the Debye-Scherrer equation, it is assumed that the peak broadening is primarily due to crystallite size and effect of microstrain is negligible. But the microstrain present in samples of nanograin size also contributes to the broadening of XRD peaks. Hence the full width at half maximum ( $\beta$ ) has to be corrected for the strain effects present in the sample grains. Hall-Williamson method is the simplest method to separate the effects of strain and grain size on the broadening of XRD peaks<sup>26, 27</sup>. Based on this method, the full width at half maximum can be written as a linear combination of the contributions from the strain ( $\epsilon$ ) and small particle size ( $D$ ) through the relation

$$\beta \cos \theta / \lambda = k/D + \epsilon \sin \theta / \lambda \quad (2)$$

$\beta \cos \theta / \lambda$  is plotted as a function of  $\sin \theta / \lambda$  and the slope of the straight line fit will give  $\epsilon$ , the residual strain, and the y-intercept will be equal to  $k/D$ , from which the crystallite size,  $D$ , may be determined. Hall Williamson plot of one of the samples of nanocrystalline  $\text{CaWO}_4$  is shown in figure 3. From the reciprocal of the y-intercept the average grain sizes were found to be 13 and 26 nm and are designated with sample codes CT1 and CT3.

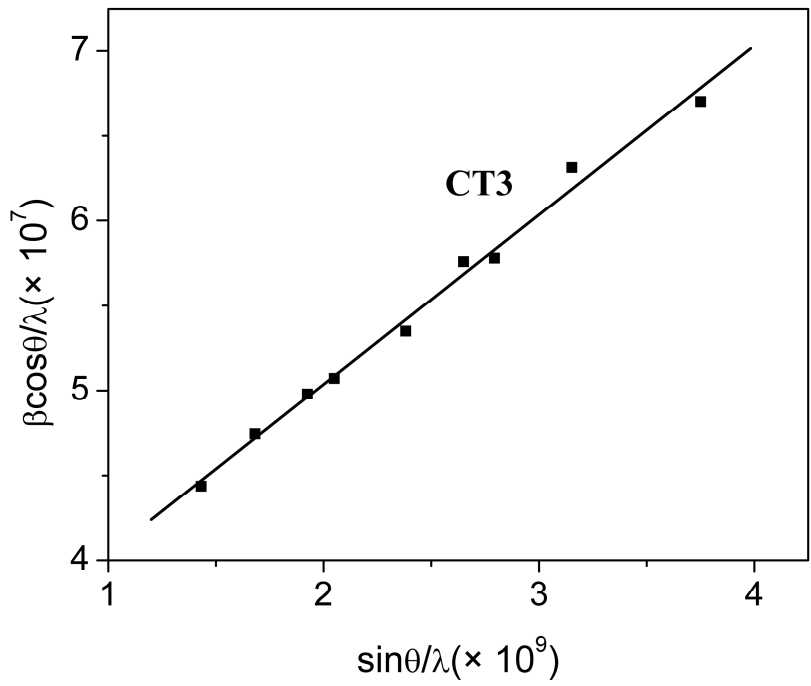
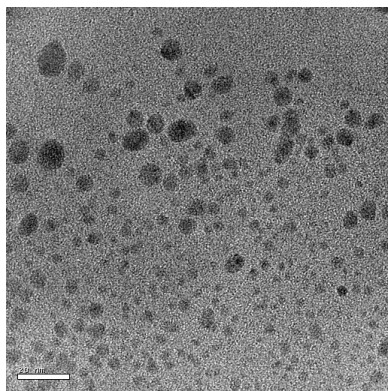
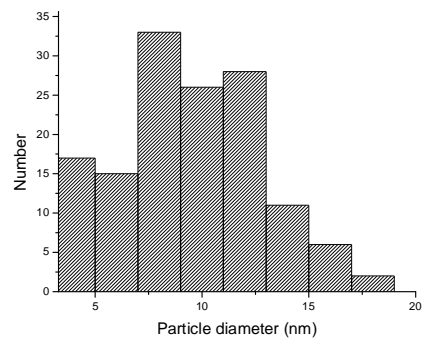


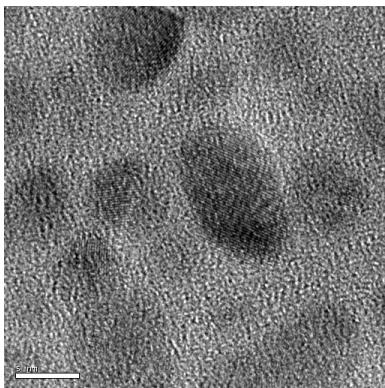
Figure 3 Hall-Williamson plot for sample CT3



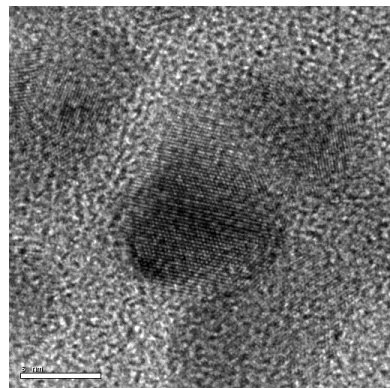
(a)



(b)



(c)



(d)

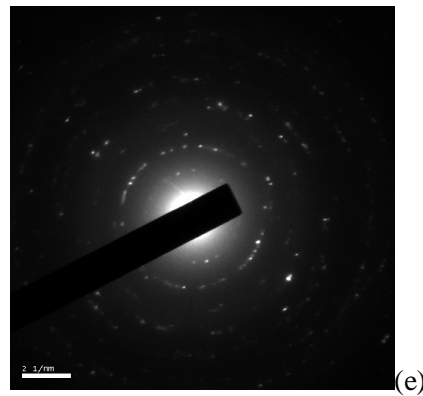


**Figure 4 (a) TEM image of nanocrystalline CaWO<sub>4</sub> (sample code – CT1) (b) particle size distribution obtained from TEM (c) and (d) high resolution TEM image of nanocrystalline CaWO<sub>4</sub> (e) electron diffraction pattern of nanocrystalline CaWO<sub>4</sub>**

Figure 4(a) shows the Transmission Electron Microscope (TEM) image of nanocrystalline calcium tungstate (sample code – CT1). TEM image indicates that most of the nanocrystals are nearly spherical in shape and some are oval in shape. Figure 4(b) is a plot of the size distribution obtained from the TEM image. It may be observed that the particle sizes range from 4-15 nm and this value agrees well with that determined using X-ray diffraction. Figure 4(c) and 4(d) show high resolution TEM image of the sample CT1. It shows lattice fringes indicating the good crystallinity of the sample. The lattice spacing of the different fringes were found to be 3.14, 1.94 and 1.85 Å which correspond to (112), (204) (220) planes respectively. Also the electron diffraction pattern of nanocrystalline CaWO<sub>4</sub> (figure 4(e)) showed sharp rings indicating the crystallinity of the sample.

In order to measure the dc conductivity of the samples, nanoparticles of CaWO<sub>4</sub> were compacted in the form of cylindrical pellets of diameter 13 mm and of thickness of 1 mm by applying uniaxial force of 0.77 GPa for five minutes using hydraulic press. All the samples were compacted under identical conditions. Conducting silver paint was applied on both sides of the pellets to serve as electrodes. The silver coated pellets were air dried for 30 minutes and then heat treated at 80 °C for 15 minutes for electrode curing. The pellets of nanostructured CaWO<sub>4</sub> with average grain size 13 nm were prepared by applying a compacting pressure 0.77 GPa (sample code: CT1). In order to study the variation of dc conductivity with grain size, nanostructured CaWO<sub>4</sub> with grain size 26 nm (sample code: CT3) were also pressed into pellets by applying the same pressure of 0.77 GPa. In order to study the effect of prolonged low temperature annealing on the dc conductivity, a pellet of the sample CT1 was heat treated for two hours and was used for dc conductivity measurements (sample code: CT12H). Conductivity measurements were performed on all the pellet samples of nanocrystalline CaWO<sub>4</sub> (sample codes: CT1, CT3 and CT12H).

Electrical measurements were carried out in a cell that could be evacuated to a vacuum of 10<sup>-4</sup> torr. Before taking the actual measurements each pellet was subjected to heat and cool runs in

order to remove any residual strain due to pelletization. The dc electrical resistance, R of the sample was measured using Keithley 2400 source meter. Before the actual measurement of resistance of the samples, voltage-current measurements were performed to check the ohmic nature of electrical contacts with the samples. The voltage-current behaviour of the samples was measured by applying different voltages to the sample and measuring the current through the sample. The resistance of the sample was measured by applying a voltage corresponding to the straight line region of the V-I graph. The electrical measurements were performed for different temperatures and the dc resistance value was measured at different temperatures at intervals of 10 K. Sufficient stabilization time was ensured at each temperature, which was kept constant with an accuracy of  $\pm 1$  K. No hysteresis was observed in the variation of the conductivity during heating and cooling runs. The repeatability of the measurements was found to be good. The dc conductivity of the samples were calculated using the formula  $\sigma_{dc} = d/(RA)$  where  $d$  and  $A$  are the thickness and area of cross section the cylindrical pellet respectively. The dc conductivity of as-compacted samples of nanostructured  $\text{CaWO}_4$  of average grain size 13 nm was measured in air at a vacuum of  $10^{-2}$  and  $10^{-4}$  torr and also at atmospheric pressure.

Figure 5 shows the V-I graph for pellet sample of nanostructured  $\text{CaWO}_4$  at different temperatures. The electrode-pellet interface of the nanostructured sample was found to be ohmic, as evidenced by the linear relationship between the applied dc voltage and the measured current. Figure 6 shows the variation of  $\sigma_{dc}$  against  $1000/T$  for nanoparticle compacts of  $\text{CaWO}_4$  samples measured at reduced air pressure of  $10^{-4}$ ,  $10^{-2}$  torr and atmospheric pressure. The results of the measurements are summarized in table 1. At atmospheric pressure, the value of dc conductivity of compacted pellets of nanocrystalline  $\text{CaWO}_4$  increased from  $3.68 \times 10^{-10} \Omega^{-1}\text{cm}^{-1}$  to  $9.48 \times 10^{-9} \Omega^{-1}\text{cm}^{-1}$  when the temperature was raised from 482 to 612 K. At a pressure of  $10^{-2}$  torr, the dc conductivity of the specimen increased from  $4.5 \times 10^{-11} \Omega^{-1}\text{cm}^{-1}$  to  $1 \times 10^{-10} \Omega^{-1}\text{cm}^{-1}$  as the temperature was raised from 532 to 592 K. With a pressure of  $10^{-4}$  torr, the dc conductivity increased from  $1.08 \times 10^{-12} \Omega^{-1}\text{cm}^{-1}$  to  $6.53 \times 10^{-11} \Omega^{-1}\text{cm}^{-1}$  when the temperature was increased from 492 to 622 K. Thus as the pressure is decreased there is reduction in the dc conductivity of the pellet sample. In order to study the effect of grain size on dc conductivity and its variation with temperature, conductivity measurements were performed on compacted pellets of nanoparticles of  $\text{CaWO}_4$  having two different grain sizes. The variation of  $\sigma_{dc}$  against  $1000/T$  for compacted nanoparticles of  $\text{CaWO}_4$  of two different grain sizes, 13 and 26 nm is shown in figure 7. For the pellet sample with grain size 26 nm the conductivity increased from  $4.16 \times 10^{-9} \Omega^{-1}\text{cm}^{-1}$  to  $1.02 \times 10^{-7} \Omega^{-1}\text{cm}^{-1}$  as the temperature was increased from 482 to 612 K while for the sample with grain size 13 nm the dc conductivity increased from  $3.68 \times 10^{-10} \Omega^{-1}\text{cm}^{-1}$  to  $9.48 \times 10^{-9} \Omega^{-1}\text{cm}^{-1}$  when the

temperature was increased from 482 to 612 K (Table 2). It is observed that for a particular temperature, the dc conductivity values showed an increase for the pellet sample with higher grain size compared to sample with lower grain size. DC conductivity measurements were also performed on heat treated pellet. The variation of  $\sigma_{dc}$  with temperature of unannealed and annealed compacted samples of nanostructured  $\text{CaWO}_4$  is shown in figure 8. The measured dc conductivity of nanoparticle compacts of  $\text{CaWO}_4$  heat treated for 2 hours at 300 °C, exhibited an increase from  $8.28 \times 10^{-10} \Omega^{-1}\text{cm}^{-1}$  to  $1.37 \times 10^{-8} \Omega^{-1}\text{cm}^{-1}$  as the temperature was increased from 482 to 612 K (Table 3). The conductivity of compacted nanoparticles of  $\text{CaWO}_4$  annealed for 2 hours at 300 °C showed marginal enhancement compared to unannealed pellet.

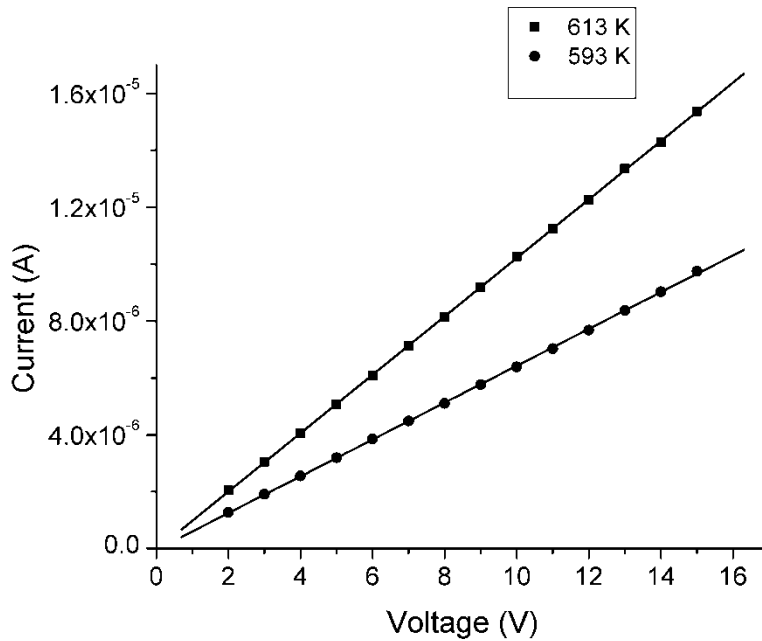


Figure 5 V-I graphs for compacted nanoparticles of  $\text{CaWO}_4$

Arrhenius behaviour, where an exponential dependence exists between the conductivity and temperature is widely reported in literature<sup>6,28,29</sup>. The temperature dependence of resistivity is given by the Arrhenius equation

$$\rho = \rho_0 \exp\left(\frac{E_a}{kT}\right) \quad (3)$$

where  $\rho_0$  is the pre-exponential factor with the dimensions of  $\Omega \text{ cm}$ ,  $k$  the Boltzmann constant,  $E_a$  is the activation energy and  $T$  is the absolute temperature. Petrov et al.<sup>30</sup> reported the electrical conduction behaviour of single crystals of  $\text{CaMoO}_4$ , which has a structure similar compared to that of  $\text{PbMoO}_4$ . From tracer diffusion studies on  $\text{CaMoO}_4$  and  $\text{CaWO}_4$  it has been shown that the diffusion of the isotope  $^{185}\text{W}$  is considerably faster than that of  $^{45}\text{Ca}$ . Also from the diffusion controlled state synthesis of  $\text{CaMoO}_4$ , it has been concluded that the mass transfer of oxygen is

faster than that of molybdenum. On the basis of this it has been assumed that oxygen ions are the most mobile ionic species in  $\text{CaMoO}_4$ . In the case of nanocrystalline  $\text{CaWO}_4$ , all the pellet samples exhibited Arrhenius behaviour. The increase in the dc conductivity with temperature is due to the increase in the thermally activated drift mobility of the charge carriers.

**Table 1** Temperature dependent variation of DC conductivity ( $\sigma_{dc}$ ) of nanocrystalline  $\text{CaWO}_4$  of average grain size 13 nm under different pressures (sample code: CT1).

10 <sup>-4</sup> torr		10 <sup>-2</sup> torr		Atmospheric pressure	
T (K)	$\sigma_{dc}$ ( $\Omega^{-1}\text{cm}^{-1}$ )	T (K)	$\sigma_{dc}$ ( $\Omega^{-1}\text{cm}^{-1}$ )	T (K)	$\sigma_{dc}$ ( $\Omega^{-1}\text{cm}^{-1}$ )
622	$6.53 \times 10^{-11}$	592	$1.00 \times 10^{-10}$	612	$9.48 \times 10^{-9}$
612	$6.12 \times 10^{-11}$	582	$9.28 \times 10^{-11}$	602	$7.92 \times 10^{-9}$
602	$5.16 \times 10^{-11}$	572	$8.80 \times 10^{-11}$	592	$6.11 \times 10^{-9}$
592	$3.77 \times 10^{-11}$	562	$6.49 \times 10^{-11}$	582	$4.77 \times 10^{-9}$
582	$2.65 \times 10^{-11}$	552	$5.60 \times 10^{-11}$	572	$3.96 \times 10^{-9}$
572	$1.75 \times 10^{-11}$	542	$4.95 \times 10^{-11}$	562	$3.21 \times 10^{-9}$
562	$1.09 \times 10^{-11}$	532	$4.50 \times 10^{-11}$	552	$2.55 \times 10^{-9}$
552	$7.26 \times 10^{-12}$			542	$1.99 \times 10^{-9}$
542	$4.85 \times 10^{-12}$			532	$1.53 \times 10^{-9}$
532	$3.15 \times 10^{-12}$			522	$1.24 \times 10^{-9}$
522	$2.22 \times 10^{-12}$			512	$9.54 \times 10^{-10}$
512	$1.96 \times 10^{-12}$			502	$7.45 \times 10^{-10}$
502	$1.53 \times 10^{-12}$			492	$6.07 \times 10^{-10}$
492	$1.08 \times 10^{-12}$			482	$3.68 \times 10^{-10}$

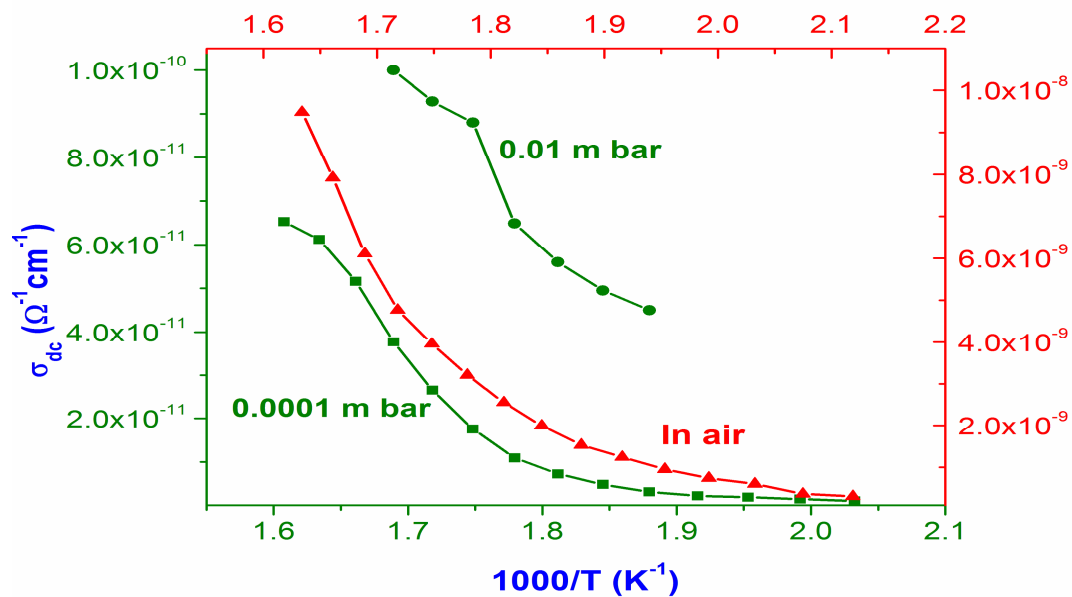


**Figure 6** Temperature dependent variation of  $\sigma_{dc}$  of nanocrystalline  $\text{CaWO}_4$  samples for different pressures (sample code: CT1)

**Table 2: Temperature dependent variation of DC conductivity ( $\sigma_{dc}$ ) of nanocrystalline  $\text{CaWO}_4$  of different average grain sizes in air**

13 nm		26 nm	
T (K)	$\sigma_{dc} (\Omega^{-1}\text{cm}^{-1})$	T (K)	$\sigma_{dc} (\Omega^{-1}\text{cm}^{-1})$
612	$9.48 \times 10^{-9}$	612	$1.02 \times 10^{-7}$
602	$7.92 \times 10^{-9}$	602	$8.03 \times 10^{-8}$
592	$6.11 \times 10^{-9}$	592	$6.40 \times 10^{-8}$
582	$4.77 \times 10^{-9}$	582	$5.03 \times 10^{-8}$
572	$3.96 \times 10^{-9}$	572	$4.10 \times 10^{-8}$
562	$3.21 \times 10^{-9}$	562	$3.21 \times 10^{-8}$
552	$2.55 \times 10^{-9}$	552	$2.52 \times 10^{-8}$
542	$1.99 \times 10^{-9}$	542	$1.85 \times 10^{-8}$
532	$1.53 \times 10^{-9}$	532	$1.44 \times 10^{-8}$
522	$1.24 \times 10^{-9}$	522	$1.13 \times 10^{-8}$
512	$9.54 \times 10^{-10}$	512	$8.45 \times 10^{-9}$
502	$7.45 \times 10^{-10}$	502	$6.74 \times 10^{-9}$
492	$6.07 \times 10^{-10}$	492	$5.27 \times 10^{-9}$
482	$3.68 \times 10^{-10}$	482	$4.16 \times 10^{-9}$

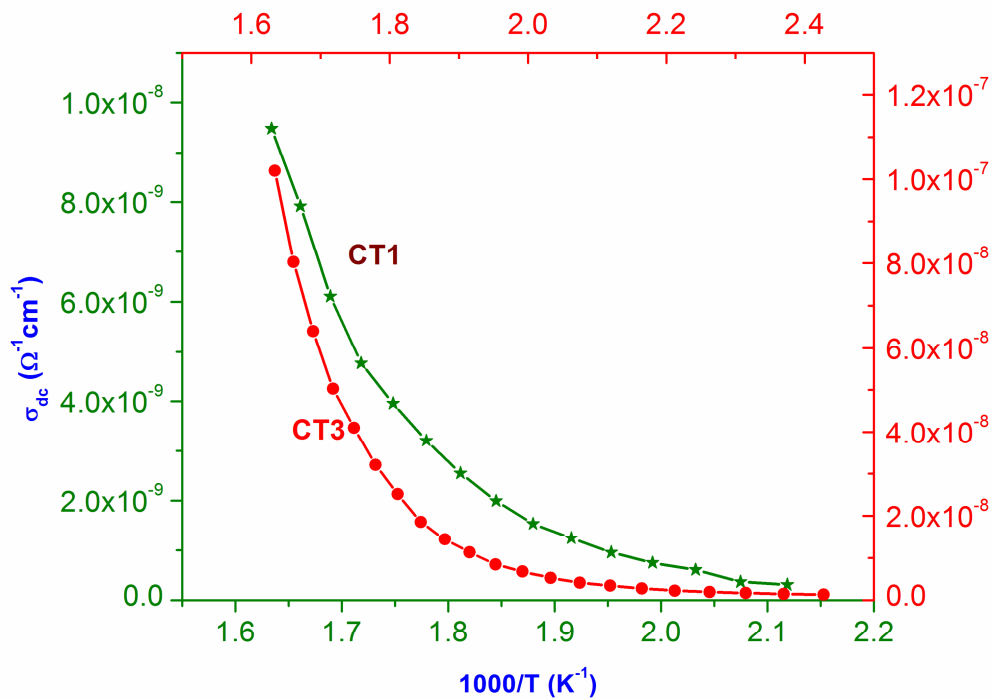


**Figure 7** Temperature dependent variation of  $\sigma_{dc}$  of nanocrystalline  $\text{CaWO}_4$  samples having different grain sizes in air. (CT1: 13 nm and CT3: 26 nm)

**Table 3: Temperature dependent variation of DC conductivity ( $\sigma_{dc}$ ) of nanocrystalline  $\text{CaWO}_4$  of average grain size 13 nm for unannealed sample and sample annealed for 2 hrs. at 300 °C in air.**

as prepared		2 hrs	
T (K)	$\sigma_{dc}$ ( $\Omega^{-1}\text{cm}^{-1}$ )	T (K)	$\sigma_{dc}$ ( $\Omega^{-1}\text{cm}^{-1}$ )
612	$9.48 \times 10^{-9}$	612	$1.37 \times 10^{-8}$
602	$7.92 \times 10^{-9}$	602	$1.17 \times 10^{-8}$
592	$6.11 \times 10^{-9}$	592	$9.99 \times 10^{-9}$
582	$4.77 \times 10^{-9}$	582	$7.70 \times 10^{-9}$
572	$3.96 \times 10^{-9}$	572	$6.73 \times 10^{-9}$
562	$3.21 \times 10^{-9}$	562	$5.49 \times 10^{-9}$
552	$2.55 \times 10^{-9}$	552	$4.18 \times 10^{-9}$
542	$1.99 \times 10^{-9}$	542	$3.17 \times 10^{-9}$
532	$1.53 \times 10^{-9}$	532	$2.61 \times 10^{-9}$
522	$1.24 \times 10^{-9}$	522	$2.14 \times 10^{-9}$
512	$9.54 \times 10^{-10}$	512	$1.67 \times 10^{-9}$
502	$7.45 \times 10^{-10}$	502	$1.36 \times 10^{-9}$
492	$6.07 \times 10^{-10}$	492	$1.05 \times 10^{-9}$
482	$3.68 \times 10^{-10}$	482	$8.28 \times 10^{-10}$

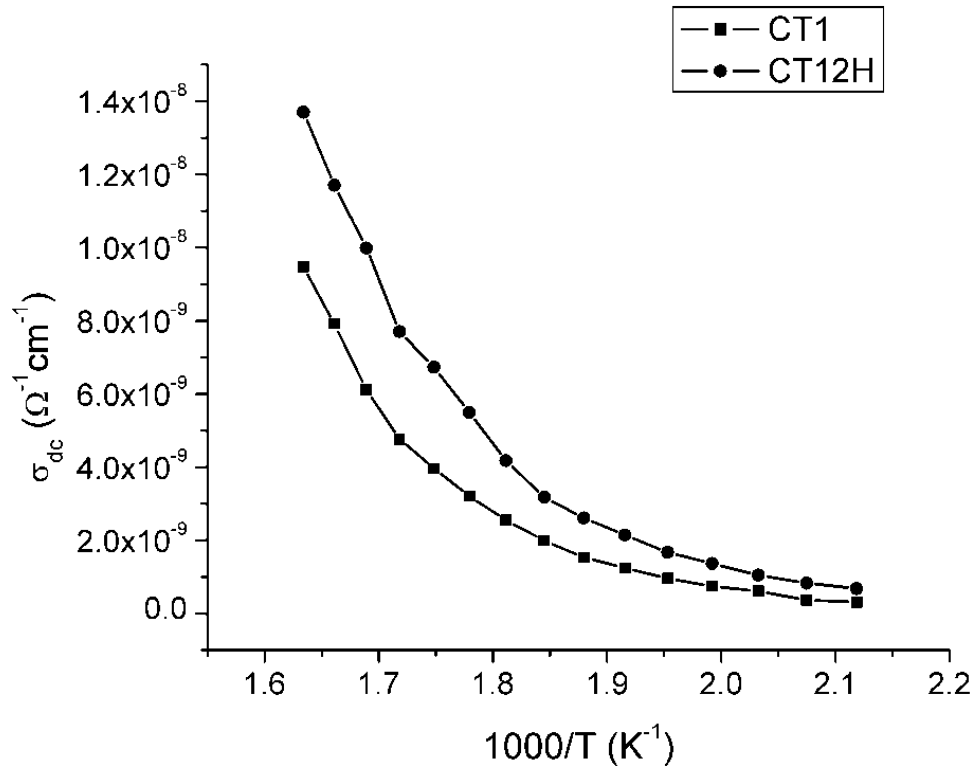


**Figure 8** Temperature dependent variation of  $\sigma_{dc}$  of unannealed and annealed nanocrystalline  $\text{CaWO}_4$  samples in air. (CT1: unannealed and CT12H: 2 hrs. annealed at 300 °C)

Density functional calculations using linearised-augmented-plane-wave method was reported for scheelite molybdates and tungstates by Zhang et. al.<sup>31</sup>. The results indicate that CaWO<sub>4</sub> has a direct band gap at the centre of the Brillouin zone. DC and ac electrical conductivities were used to characterize the type of charge transport in single crystals of CaWO<sub>4</sub> which were equilibrated with H<sub>2</sub>-H<sub>2</sub>O-Ar gas mixtures<sup>25</sup>. Measurements were made from 900° to 1300°C and at P<sub>H<sub>2</sub>O</sub>/P<sub>H<sub>2</sub></sub> ratios from 0.02 to 3.0. The ac conductivity at 1000°C varied from 51.4×10<sup>-6</sup> to 5.89×10<sup>-6</sup> mho/cm for P<sub>H<sub>2</sub>O</sub>/P<sub>H<sub>2</sub></sub>=0.02 and 2.0, respectively; the dc conductivity changed from 51.0 ×10<sup>-6</sup> to 5.42 ×10<sup>-6</sup> mho/cm under the same experimental conditions<sup>25</sup>. The results were described by a paired-defect model of oxygen vacancies and oxygen interstitials. In the present study, it was observed that for compacted nanoparticles of CaWO<sub>4</sub> the dc electrical conductivity was about two orders of magnitude lesser compared to that reported for single crystals of CaWO<sub>4</sub>. In the case of compacted nanoparticles of CaWO<sub>4</sub> the dc electrical conductivity values increased with increase in temperature. This is in agreement with already reported behaviour of variation of electrical conductivity with temperature for single crystals of CaWO<sub>4</sub>.

The optical properties like the absorption, photoluminescence and reflectance spectra exhibited by CaWO<sub>4</sub> are described in terms of charge transfer transitions in the WO<sub>4</sub><sup>2-</sup> tetrahedra<sup>22, 23</sup>. Conductivity measurements indicated that the dc conductivity of as compacted pellets of nanoparticles of CaWO<sub>4</sub> is sensitive to air pressure (Table 1). There is a possibility of presence of large fraction of surface defects in the form of oxygen vacancies in the pellet sample. These surface defects play a crucial role in determining the conductivity of the pellet sample. In the presence of air, these oxygen vacancies will be replenished to form the correct stoichiometry. The dc conductivity of nanocrystalline CaWO<sub>4</sub> pellet sample with grain size 26 nm was found to be increased compared to pellet sample with grain size 13 nm (Table 2). It is well known that the band gap of a material increases with reduction in grain size<sup>27</sup>. This phenomenon of quantum size effect is widely reported in literature<sup>27, 32, 33</sup>. This phenomenon and its impact on the optical properties is reported in the case of nanostructured CaWO<sub>4</sub><sup>34-38</sup>. As a result of widening of band gap, more energy is needed for creating free charge carriers. The band gap of nanocrystalline CaWO<sub>4</sub> of grain size 13 nm is larger compared to the sample with grain size 26 nm. It is seen that the conductivity of compacted nanoparticles of CaWO<sub>4</sub> of grain size 13 nm is marginally enhanced with heat treatment of the pellet in air at a temperature of 300 °C for 2 hours compared to unannealed pellet (Table 3). The annealing temperature was specifically kept low so that no appreciable grain growth occurs. The change observed in the dc conductivity of the sample is due to factors other than grain growth. This low temperature annealing in air can introduce significant changes in the density of defects such as interstitials, vacancies, dislocations and distribution of pores and voids. These can influence

the dc conductivity of the specimen considerably. The conductivity of annealed pellet sample was found to have a marginal increase compared to that of unannealed pellet sample. The value of conductivity at 612 K recorded an increase from  $9.48 \times 10^{-9} \Omega^{-1} \text{cm}^{-1}$  for the unannealed pellet to  $1.17 \times 10^{-8} \Omega^{-1} \text{cm}^{-1}$  for the pellet heat treated for 2 hours (Table 3). Upon heat treatment, the pore density of the specimen reduced and the pellet become more rigid compared to unannealed pellets resulting in better contacts between individual grains. This may be the possible reason of enhancement of conductivity of the heat treated pellet samples of  $\text{CaWO}_4$ .

## **CONCLUSION**

Nanocrystalline calcium tungstate of two different grain sizes 13 and 26 nm were synthesized using aqueous chemical precipitation method. The crystal structure and grain size of different samples were determined using x-ray diffraction data. The effect of microstrain on broadening of X-ray diffraction peak was eliminated using Hall-Williamson analysis. Transmission electron microscopy was also used to estimate the particle size distribution and morphology. The lattice planes were clearly visible in high resolution transmission electron microscope images indicating good crystallinity of the samples in agreement with XRD analysis. The interplanar spacings measured from HRTEM images agree well with the data obtained from X-ray diffraction patterns. The sharp rings obtained in the electron diffraction pattern showed that the samples were crystalline.

DC conductivity measurements were done on compacted pellets of nanocrystalline samples of  $\text{CaWO}_4$ . It was found that the dc conductivity showed an exponential increase with temperature exhibiting Arrhenius behaviour for all the samples. For nanoparticle compacts of  $\text{CaWO}_4$ , the measured dc conductivity was about two orders of magnitude less than that reported for single crystals of  $\text{CaWO}_4$ . Also, the dc conductivity showed an increase with increase in average grain size of the sample. The conductivity measurements performed on pellet heat treated for two hours at a low temperature of  $300^\circ\text{C}$  exhibited enhancement in dc conductivity compared to unannealed green pellet. This enhancement as a result heat treatment may be due to reduction of porosity which results in better contact between grains.

**ACKNOWLEDGEMENT:** The author acknowledges the guidance given by Prof. M Abdul Khadar, Professor (Emeritus) Centre for Nanoscience and Nanotechnology, University of Kerala. This study is done with the assistance of University Grants Commission under FIP and DST, NSTI.

## REFERENCES

1. Mohanraj VA, Chen Y. Nanoparticles – A review. *Trop. J. Pharma. Res.* 2006; 5(1): 561-573.
2. Clemens B, Xiaoba C, Radha N, Mostafa AE. Chemistry and properties of nanocrystals of different shapes. *Chem. Rev.* 2005; 125: 1025.
3. Xuebin Y, Zeiwi T, Dalin S, Liuzhang O, Min Z. Recent advances and remaining challenges of nanostructured materials for hydrogen storage applications. *Prog. Mater. Sci.* 2017; 88: 1.
4. Ovidko IA, Valiev RZ, Zhu YT. Review on superior strength and enhanced ductility of metallic nanomaterials. *Prog. Mater. Sci.* 2018; 94: 462-540.
5. Ukoba KO, Eloka-Eboka AC, Inambao FL. Review of nanostructured NiO thin film using the spray pyrolysis technique. *Renew. Sust. Energy Rev.* 2018; 82: 2900-2915.
6. Biju V, Abdul Khadar M. DC conductivity of consolidated nanoparticles of NiO. *Mater. Res. Bull.* 2001; 36: 21-33.
7. Matthew RD, Joshua M, George SN, Ayusman S, John VB. Thermal and electrical conductivity of bismuth telluride nanoparticles. *Small* 2009; 5: 933-937.
8. Saafan SA, Meas TM, El-Ghazzawy EH et al. AC and DC conductivity of NiZn ferrite nanoparticles in wet and dry conditions. *J. Magn. Mater.* 2010; 322: 2369-2374.
9. Bargougui R, Bouazizi N, Ben Soltan W et al. Controlled synthesis and electrical conduction properties of anatase TiO<sub>2</sub> nanoparticles via polyol method. *Appl. Phys. A* 2016; 22: 309.
10. Shobhna C. Structural, morphological, thermal, dielectric and electrical properties of alumina nanoparticles of filled PVA-PVP blend matrix-based polymer nanocomposites. *Polym. Compos.* 2018; 39: E1788-E1799.
11. Chiang YM, Lavik EB, Blom DA. Defect thermodynamics and electrical properties of nanocrystalline oxides : pure and doped CeO<sub>2</sub>. *Nanostruct. Mater.* 1997; 9: 633-642.
12. Lu K, Wang JT, Wei WD. Comparison of properties of nanocrystalline and amorphous Ni-P alloys. *J. Phys. D: Appl. Phys.* 1998; 25: 808.
13. Sivakumar N, Narayanasamy A, Shinoda K, Chinnasamy CN, Jeyadevan B. Electrical and magnetic properties of chemically derived nanocrystalline cobalt ferrite. *J. Appl. Phys.* 2007;10: 013916.
14. Abdulkhadar M, Binny Thomas. DC conductivity of nanoparticles of CdS and ZnS. *Nanostruct. Mater.* 1998; 10: 593-600.

15. Brus L. Electronic wave functions in semiconductor clusters: Experiment and Theory. *J. Phys. Chem.* 1986; 90: 2555-2560.
16. Lijuan C, Liping L, Guangshe L. Surface hydration-mediated conduction of NiO nanocrystals. *Solid State Ion.* 2008; 179: 712-717.
17. Anindita B, Soumen B, Sourish B, Dipankar .C. Electrical properties of compacted assembly of copper oxide nanoparticles. *J. Appl. Phys.* 2005; 98: 074307.
18. Das D, Chakravorty D. Interfacial conduction in silica gels containing nanocrystalline copper oxide. *Appl. Phys. Lett.* 2000; 76: 1273.
19. Nan C, Tschope A, Holten S, Kleim H, Birringer R. Grain-size dependent electrical properties of nanocrystalline ZnO. *J. Appl. Phys.* 1999; 85: 7735.
20. Babita B, Kishore Kumar D, Manorama SV. Hydrothermal synthesis of highly crystalline ZnO nanoparticles : A competitive sensor for LPG and EtOH. *Sens. Actu. B : Chem.* 2006; 119: 676-682.
21. Porto SPS, Scott JF. Raman Spectra of  $\text{CaWO}_4$ ,  $\text{SrWO}_4$ ,  $\text{CaMoO}_4$  and  $\text{SrMoO}_4$ . *Phys. Rev.* 1967; 157(3): 716.
22. Treadway MJ, Powell RC. Luminescence of calcium tungstate crystals. *J. Chem. Phys.* 1974; 61: 4003.
23. Grasser R, Pitt E, Zimmerer G. Optical properties of  $\text{CaWO}_4$  and  $\text{CaMoO}_4$  crystals in the 4 to 25 eV region. *Phy. Stat. Sol., (b)* 1975; 69: 359-368.
24. Groenink JA, Binsma H. Electrical conductivity and defect chemistry of  $\text{PbMoO}_4$  and  $\text{PbWO}_4$ . *J. Sol. State Chem.* 1979; 29: 227-236.
25. Rigdon MA, Grace RE. Electrical charge transport in single-crystal  $\text{CaWO}_4$ . *J. Amer. Ceram. Soc.* 1979; 29: 227.
26. Williamson GK, Hall WH. X-ray line broadening from filed aluminium and wolfram. *Acta Metall.* 1953; 1: 22-31.
27. Anandakumar VM, Abdul Khadar M. Synthesis, characterization and optical properties of nanocrystalline lead molybdate. *Phys. Stat. Sol. (a)* 2008; 205: 2666-2672.
28. Balachandran U, Eror NG. Electrical conductivity in strontium titanate. *J. Solid State Chem.* 1981; 39: 351-359.
29. Rhimi T, Leroy G, Duponchal B, Khirouni K, Guerhazi S, Toumi M. AC and DC conductivity studies of  $\text{LiH}_2\text{PO}_4$  compound using impedance spectroscopy. *Ionics* 2018; 24: 1305-13012.
30. Petrov A, Kofstad P. Electrical conductivity of  $\text{CaMoO}_4$ . *J. Sol. State Chem.* 1979; 30: 83-88.

31. Zhang Y, Holzwarth NAW, Williams RT. Electronic band structures of the scheelite materials  $\text{CaMoO}_4$ ,  $\text{CaWO}_4$ ,  $\text{PbMoO}_4$  and  $\text{PbWO}_4$ . *Phys. Rev. B* 1998; 57: 12738-12750.
32. Rajeev RP, Abdul Khadar M. Characterization of chemically synthesized CdS nanoparticles. *Pramana – J. Phys.* 2005; 65: 801-807.
33. Kanade KG, Kale BB, Aiyer RC, Das BK. Effect of solvents on the synthesis of nano-size zinc oxide and its properties. *Mater. Res. Bull.* 2006; 41: 590-600.
34. Lou Z, Cocivera M. Cathodoluminescence of  $\text{CaWO}_4$  and  $\text{SrWO}_4$  thin films prepared by spray pyrolysis. *Mater. Res. Bull.* 2002; 37: 1573-1582.
35. Chen D, Guozhen S, Kaibin T, Huagui Z, Yitai Q. Low temperature synthesis of metal tungstates nanocrystallites in ethylene glycol. *Mater. Res. Bull.* 2003; 38: 1783-1789.
36. Cavalcante LS, Longo VM, Sczancoski JC, Almada MAP et al. Electronic structure, growth mechanism and photoluminescence of  $\text{CaWO}_4$  crystals. *CrystEngComm* 2012; 14: 853-868.
37. Valeria ML, Lourdes G, Daniel GS et al. A joint experimental and theoretical study of nanomorphology of  $\text{CaWO}_4$  crystals. *J. Phys. Chem.* 2011; 115: 20113-20119.
38. Thongtem T, Phuruangrat A and Thongtem S. Synthesis of  $\text{CaWO}_4$ ,  $\text{SrWO}_4$  and  $\text{BaWO}_4$  with nanosized particles using cyclic microwave radiation. *J. Ceram. Proc. Res.* 2008; 9(3): 258-2661.